AFRL-RB-WP-TP-2011-3105

DYNAMICS AND CONTROL OF A MINIMALLY ACTUATED BIOMIMETIC VEHICLE: PART I - AERODYNAMIC MODEL (POSTPRINT)

David B. Doman, Michael W. Oppenheimer, and David O. Sigthorsson

Control Design and Analysis Branch
Control Sciences Division

AUGUST 2009

AIR FORCE RESEARCH LABORATORY
AIR VEHICLES DIRECTORATE
WRIGHT-PATTERSON AIR FORCE BASE, OH 45433-7542
AIR FORCE MATERIEL COMMAND
UNITED STATES AIR FORCE

REPORT DOCUMENTATION PAGE

Form Approved
OMB No. 0704-0188

1. REPORT DATE *(DD-MM-YY)*	2. REPORT TYPE	3. DATES COVERED *(From - To)*
August 2009	Conference Paper Postprint	05 November 2008 – 13 August 2009

4. TITLE AND SUBTITLE
DYNAMICS AND CONTROL OF A MINIMALLY ACTUATED BIOMIMETIC VEHICLE: PART I - AERODYNAMIC MODEL (POSTPRINT)

5a. CONTRACT NUMBER
In-house

5b. GRANT NUMBER

5c. PROGRAM ELEMENT NUMBER
62201F

6. AUTHOR(S)
David B. Doman, Michael W. Oppenheimer, and David O. Sigthorsson (AFRL/RBCA)

5d. PROJECT NUMBER
2401

5e. TASK NUMBER
N/A

5f. WORK UNIT NUMBER
Q12K

7. PERFORMING ORGANIZATION NAME(S) AND ADDRESS(ES)
Control Design and Analysis Branch (AFRL/RBCA)
Control Sciences Division
Air Force Research Laboratory, Air Vehicles Directorate
Wright-Patterson Air Force Base, OH 45433-7542
Air Force Materiel Command, United States Air Force

8. PERFORMING ORGANIZATION REPORT NUMBER
AFRL-RB-WP-TP-2011-3105

9. SPONSORING/MONITORING AGENCY NAME(S) AND ADDRESS(ES)
Air Force Research Laboratory
Air Vehicles Directorate
Wright-Patterson Air Force Base, OH 45433-7742
Air Force Materiel Command
United States Air Force

10. SPONSORING/MONITORING AGENCY ACRONYM(S)
AFRL/RBSD

11. SPONSORING/MONITORING AGENCY REPORT NUMBER(S)
AFRL-RB-WP-TP-2011-3105

12. DISTRIBUTION/AVAILABILITY STATEMENT
Approved for public release; distribution unlimited.

13. SUPPLEMENTARY NOTES
PAO Case Number: 88ABW-2009-3584; Clearance Date: 10 Aug 2009. Document contains color.

Conference paper published in the proceedings of the AIAA Guidance, Navigation, and Control Conference held 10 - 13 August 2009 in Chicago, IL.

14. ABSTRACT
An aerodynamic model for the forces and moments acting on a minimally actuated flapping wing micro air vehicle (FWMAV) are derived from blade element theory. The proposed vehicle is similar to the Harvard RoboFly that accomplished the first takeoff of an insect scale flapping wing aircraft, except that it is equipped with independently actuated wings and the vehicle center-of-gravity can be manipulated for control purposes. Using a blade element-based approach, both instantaneous and cycle-averaged forces and moments are computed for a specific type of wing beat motion that enables nearly decoupled, multi-degree-of-freedom control of the aircraft. The wing positions are controlled using oscillators whose frequencies change once per wing beat cycle. A new technique is introduced, called Split-Cycle Constant-Period Frequency Modulation, that has the desirable property of providing a high level of control input decoupling for vehicles without active angle-of-attack control. Like the RoboFly, the wing angle-ofattack variation is passive by design, and is a function of the instantaneous angular velocity of the wing in the stroke plane. A control-oriented dynamic model of the vehicle is derived, which is based on a cycle-averaged representation of the forces and moments. Control derivatives are calculated and a cycle-averaged control law is designed that provides control over 5 degrees-of-freedom of the vehicle.

15. SUBJECT TERMS
flapping wing micro air vehicles, MAV, flapping wing aerodynamic model, blade element theory, Split-Cycle Constant-Period Frequency Modulation

16. SECURITY CLASSIFICATION OF:			17. LIMITATION OF ABSTRACT:	18. NUMBER OF PAGES	19a. NAME OF RESPONSIBLE PERSON (Monitor)
a. REPORT	b. ABSTRACT	c. THIS PAGE			1Lt Zachary H. Goff
Unclassified	Unclassified	Unclassified	SAR	32	19b. TELEPHONE NUMBER *(Include Area Code)* N/A

AIAA Guidance, Navigation, and Control Conference
10 - 13 August 2009, Chicago, Illinois

AIAA 2009-6160

Dynamics and Control of a Minimally Actuated Biomimetic Vehicle:

Part I - Aerodynamic Model

David B. Doman *

Michael W. Oppenheimer †

David O. Sigthorsson ‡

An aerodynamic model for the forces and moments acting on a minimally actuated flapping wing micro air vehicle (FWMAV) are derived from blade element theory. The proposed vehicle is similar to the Harvard RoboFly that accomplished the first takeoff of an insect scale flapping wing aircraft, except that it is equipped with independently actuated wings and the vehicle center-of-gravity can be manipulated for control purposes. Using a blade element-based approach, both instantaneous and cycle-averaged forces and moments are computed for a specific type of wing beat motion that enables nearly decoupled, multi-degree-of-freedom control of the aircraft. The wing positions are controlled using oscillators whose frequencies change once per wing beat cycle. A new technique is introduced, called Split-Cycle Constant-Period Frequency Modulation, that has the desirable property of providing a high level of control input decoupling for vehicles without active angle-of-attack control. Like the RoboFly, the wing angle-of-attack variation is passive by design, and is a function of the instantaneous angular velocity of the wing in the stroke plane. A control-oriented dynamic model of the vehicle is derived, which is based on a cycle-averaged

*Senior Aerospace Engineer, Control Design and Analysis Branch, 2210 Eighth Street, Ste. 21, Air Force Research Laboratory, WPAFB, OH 45433-7531 Email David.Doman@wpafb.af.mil, Ph. (937) 255-8451, Fax (937) 656-4000, Associate Fellow AIAA

†Senior Electronics Engineer, Control Design and Analysis Branch, 2210 Eighth Street, Ste 21, Air Force Research Laboratory, WPAFB, OH 45433-7531 Email Michael.Oppenheimer@wpafb.af.mil, Ph. (937) 255-8490, Fax (937) 656-4000, Senior Member, AIAA

‡Electronics Engineer, Control Design and Analysis Branch, 2210 Eighth Street, Ste 21, Air Force Research Laboratory, WPAFB, OH 45433-7531 Email David.Sigthorsson@afmcx.net, Ph. (937) 255-9707, Fax (937) 656-4000. This research was performed while this author held a National Research Council Research Associateship Award at the Air Force Research Laboratory.

representation of the forces and moments. Control derivatives are calculated and a cycle-averaged control law is designed that provides control over 5 degrees-of-freedom of the vehicle.

I. Introduction

The first takeoff of an insect-scale flapping wing micro air vehicle was achieved by an aircraft called RoboFly that was developed at Harvard University by Wood et.al.[1] A key feature that led to the successful first flight is that the vehicle was minimally actuated. RoboFly uses a single bimorph piezoelectric actuator to impart symmetric stroke plane motion to two wings. The wing angle-of-inclination with respect to the stroke plane is passively regulated by wing flexure joints resulting in planform motion that is similar to that of a dipterian insect. This passive rotation of the planform about the spar eliminates the need for added weight and complexity associated with actuators that actively rotate the planform about the spar. The first flight at Harvard resulted in unregulated flight up a pair of wires that constrained the vehicle motion to vertical translation.

In the present paper, a vehicle concept and a control strategy, that would enable controlled six-degree-of-freedom flight of the fuselage of an aircraft similar to the RoboFly without the need for artificial motion constraints, are developed. A diagram of the proposed vehicle is shown in Figure 1.

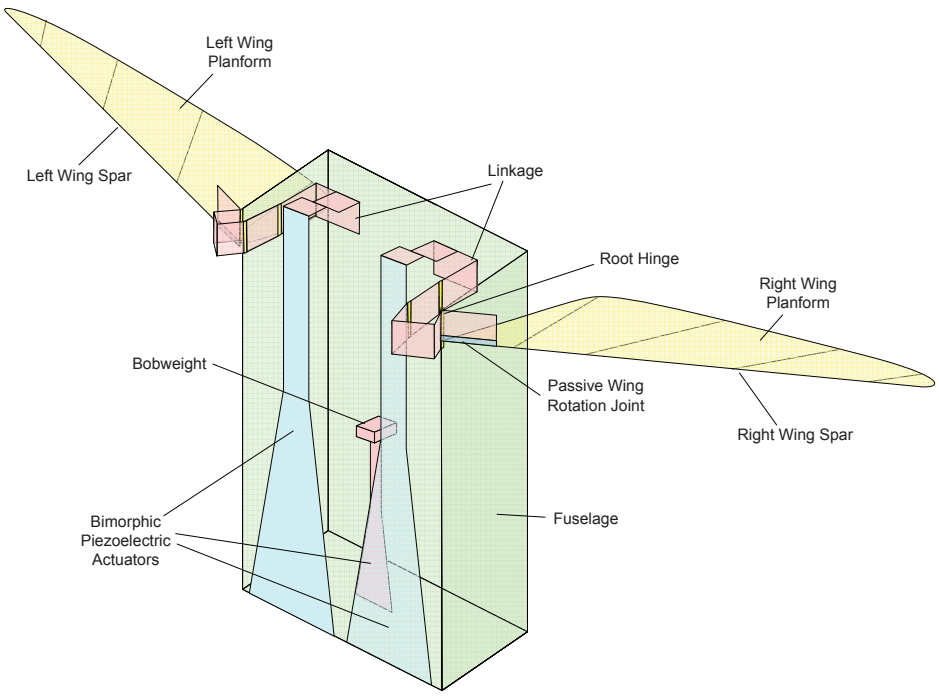

Figure 1. General assembly of a minimally actuated flapping wing micro air vehicle.

The differences between the proposed aircraft and the Harvard RoboFly are that it would be equipped with independently actuated wings and an actuated bob-weight that would allow the vehicle center-of-gravity to be manipulated for control purposes. The wings rotate about hinges at the wing root. A linkage based transmission translates the tangential motion of the tip of a bimorph piezoelectric actuator into rotational motion of the wings in the stroke plane. The linkage elements are designed to achieve impedance matching between the wing and actuator forces as well as amplify the relatively small motion of the tip of the bimorph strip into large angular displacements of the wing root. The planforms are connected to the movable wing roots by a limited hinge joint that provides for passive rotation of the wing. This hinge allows the wing to passively flip-over as the wing reverses direction at the end of each stroke and enables the chord to rotate about the axis of the spar in a manner that approximates the wing-twisting motion that has been observed in dipterian insects.[2] As the wing rotates through the stroke plane, dynamic pressure acting on the wing tends to cause it to feather into the wind; however, as shown in Figure 2, the spar and root structure interfere at an angle set by the designer to prevent the wing from over-rotating. This interference causes the wing to hold a constant angle-of-attack relative to the stroke plane once a critical dynamic pressure is reached.

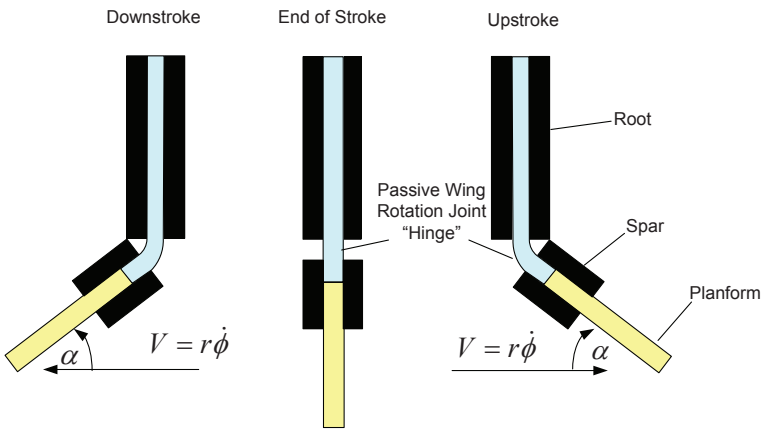

Figure 2. Detail of passive wing rotation joint.

The bimorph piezoelectic actuators and the carbon fiber substrate to which they are mounted are cantilevered to the fuselage. In the case of the wings, the actuator assembly and linkage, together with the wing, form a spring-mass-damper system that has a known resonant frequency. The actuator assembly for the bob-weight is simply used to control the mean pitch attitude of the fuselage. In the single actuator Harvard experiments, the dynamic system was driven at resonance[3] for maximum energy efficiency to achieve flight. In the present problem, each wing-linkage-actuator system is nominally driven at a hover frequency that is defined as the frequency at which the cycle-averaged lift is equal to the weight of the aircraft. The term hover is to be interpreted in a time-averaged sense because as we will show, the aircraft is in constant motion due to the periodic nature of the forces and moments produced by the flapping wings. The closest approximation of hover that can be achieved is that of a high frequency, low amplitude limit cycle about a mean position.[4]

Using a blade element based aerodynamic model and time averaging, it will be shown that 5 independent degrees of freedom can be controlled and that the 6th degree-of-freedom can be manipulated by coordinated motion of a subset of the 5 degrees of freedom. The wing angle-of-attack variation is passive and is a function of the instantaneous angular velocity of the wing in the stroke plane. The control laws are therefore designed to make use of three actuators, two of which control the angular position of the wing in the stroke plane and one that moves a bob-weight that manipulates the vehicle center-of-gravity. A technique called Split-Cycle Constant-Period Frequency Modulation is proposed that allows each wing to generate non-zero cycle-averaged rolling and yawing moments as well as translational forces that can accelerate the vehicle forwards and backwards while maintaining a wingbeat forcing function that keeps the wing-actuator dynamics operating near the hover frequency. The split-cycle technique achieves this objective by varying the frequency of the oscillators that drive the wing position actuators, such that the dynamic pressure acting on the wing during

the forestroke is different from that acting on the aftstroke. Pitching moment and high speed translation are controlled by varying the vehicle center-of-gravity.

A. Preliminary Assumptions

The purpose of this investigation is to derive an idealized model that will allow one to study the dynamic behavior of the aircraft under consideration and to formulate and test control strategies using non-real-time simulations. This objective limits the fidelity of the aerodynamic and structural models that can be used. The use of computational fluid dynamics and finite element structural codes would be computationally intractable for a simulation of this type and would likely impede physical insights that would allow one to formulate a control law and observe key vehicle design features. In light of the above objective, the following assumptions are made:

- There are no aerodynamic interactions between the left and right wings.
- There are no aerodynamic interactions between the wings and the fuselage.
- The 2D sectional aerodynamic coefficients are known and constant throughout each stroke. Three dimensional and unsteady effects from leading edge vortex and wake phenomena are not present.
- The passive wing rotation joint is on a limit when the wing angular velocity in the stroke plane is non-zero.
- The air mass surrounding the vehicle is quiescent.
- Aerodynamic forces and moments are the sole result of wing motion, i.e., only flight conditions in the neighborhood of hover are considered.
- The bandwidth of the piezoelectric actuators exceeds the hover frequency.

II. Coordinate Frame Definitions

The dynamic analysis of the vehicle requires the use of several coordinate frames. This is because the signs of aerodynamic forces and moments differ from the right wing to the left. Furthermore, the signs of the forces and moments are dependent upon the direction of the wing stroke, i.e., upstroke or downstroke. The aerodynamic forces and moments can be conveniently written in certain intermediate frames; however, it will be necessary to transform these parameters into a body-fixed and ultimately an inertial coordinate frame in order to write the equations of motion of the fuselage. Definitions of the numerous

coordinate frames and rotation matrices required in this analysis are provided in Tables 1 and 2, respectively. The coordinate frame and angle definitions are illustrated in Figure 3.

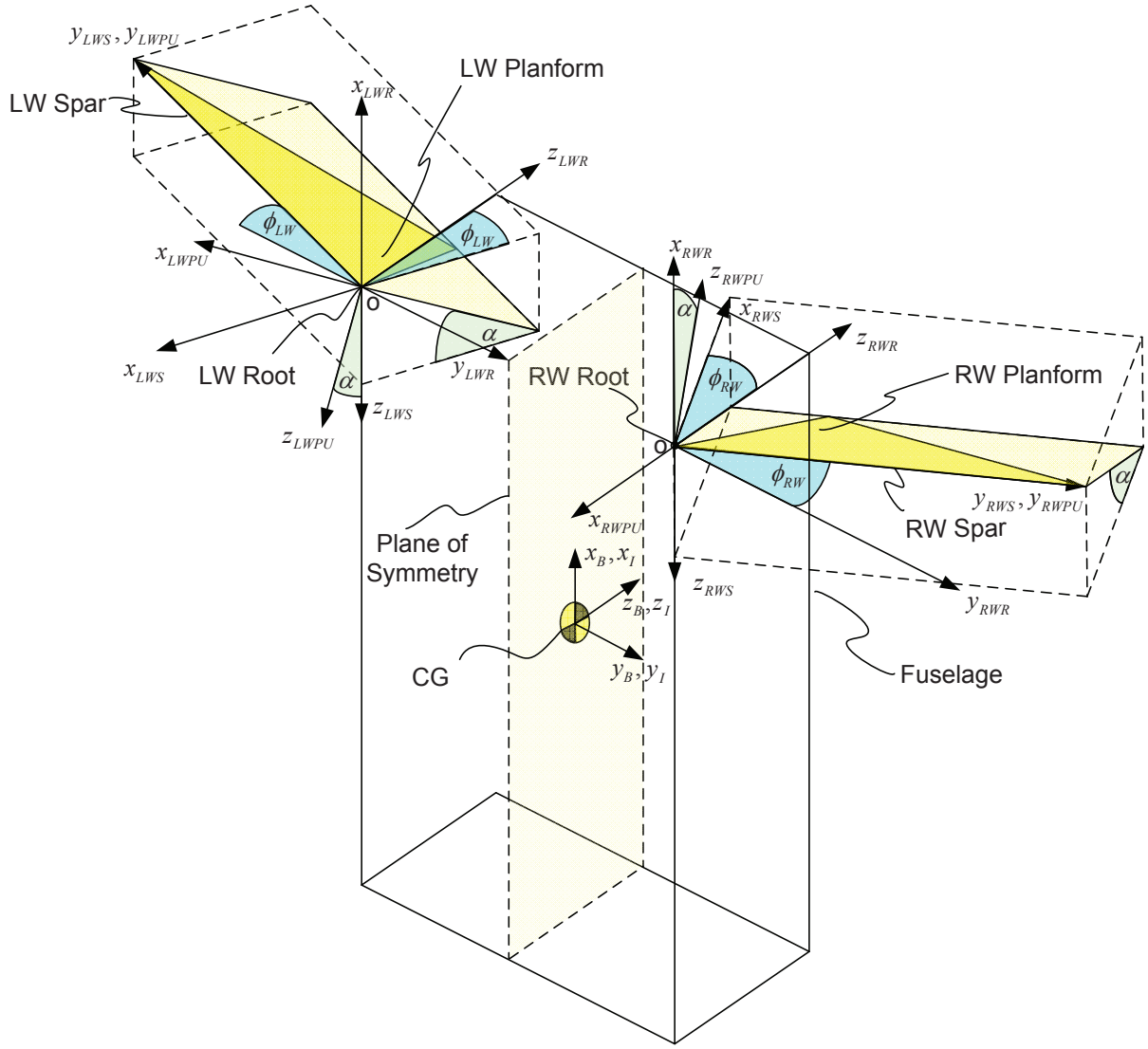

Figure 3. Relationship between, body, root, spar, left and right wing planform axis systems on upstroke.

A system of notation has been selected where superscripts "cancel" subscripts when multiplying rotation matrices. For vector quantities, superscripts identify the coordinate frame in which the quantities are expressed, while subscripts identify the quantity.

Frame	Symbol	Feature	Location/Sense
Body (Fixed to Fuselage)	B	Origin	Nominal Center of Gravity
		x_B axis	(+) Anterior Normal to Stroke Plane
		y_B axis	(+) Right Hand Side
		z_B axis	(+) Ventral Side
Inertial (Fixed to Flat Earth)	I	Origin	Initially Coincident with Body Center-of-Gravity
		x_I axis	(+) Initially Aligned with x_B axis
		y_I axis	(+) Initially Aligned with y_B axis
		z_I axis	(+) Initially Aligned with z_B axis
RW Root (Fixed to Fuselage)	RWR	Origin	RW Root Hinge Point
		x_{RWR} axis	(+) in x_B dir.
		y_{RWR} axis	(+) in y_B dir.
		z_{RWR} axis	(+) in z_B dir.
LW Root (Fixed to Fuselage)	LWR	Origin	LW Root Hinge Point
		x_{LWR} axis	(+) in x_B dir.
		y_{LWR} axis	(+) in y_B dir.
		z_{LWR} axis	(+) in z_B dir.
RW Spar (Rotates with RW Spar)	RWS	Origin	RW Root Hinge Point
		x_{RWS} axis	(+) Towards ventral side at $\phi_{RW} = 0$
		y_{RWS} axis	(+) Proximal to distal, coincident $\overline{c}$ RW spar
		z_{RWS} axis	(+) Towards posterior of fuselage
LW Spar (Rotates with LW Spar)	LWS	Origin	LW Root Hinge Point
		x_{LWS} axis	(+) Towards dorsal side at $\phi_{LW} = 0$
		y_{LWS} axis	(+) Proximal to distal, coincident $\overline{c}$ spar
		z_{LWS} axis	(+) Towards posterior of fuselage
RW Planform Upstroke (Aligned $\overline{c}$ RW Plane on Upstroke)	RWPU	Origin	RW Root Hinge Point
		x_{RWPU} axis	(+) Direction of wing rotation
		y_{RWPU} axis	(+) Proximal to distal, coincident $\overline{c}$ RW spar
		z_{RWPU} axis	(+) anterior, completes RH coord. sys
RW Planform Downstroke (Aligned $\overline{c}$ RW Plane on Downstroke)	RWPD	Origin	RW Root Hinge Point
		x_{RWPD} axis	(+) Direction of wing rotation
		y_{RWPD} axis	(+) Proximal to distal, coincident $\overline{c}$ RW spar
		z_{RWPD} axis	(+) posterior, completes RH coord. sys
LW Planform Upstroke (Aligned $\overline{c}$ LW Plane on Upstroke)	LWPU	Origin	LW Root Hinge Point
		x_{LWPU} axis	(+) Direction of wing rotation
		y_{LWPU} axis	(+) Proximal to distal, coincident $\overline{c}$ LW spar
		z_{LWPU} axis	(+) posterior, completes RH coord. sys
LW Planform Downstroke (Aligned $\overline{c}$ LW Plane on Downstroke)	LWPD	Origin	LW Root Hinge Point
		x_{LWPD} axis	(+) Direction of wing rotation
		y_{LWPD} axis	(+) Proximal to distal, coincident $\overline{c}$ LW spar
		z_{LWPD} axis	(+) anterior, completes RH coord. sys

Table 1. Coordinate Frame Definitions.

From	To	Stroke	Symbol	Rotation Matrix
RW & LW Root	Body	Either	R^B_R	$R^B_{RWR} = R^B_{LWR} = \mathbf{I}$
RW Spar	RW Root	Either	R^{RWR}_{RWS}	$\begin{bmatrix} 0 & 0 & -1 \\ -\sin\phi_{RW} & \cos\phi_{RW} & 0 \\ \cos\phi_{RW} & \sin\phi_{RW} & 0 \end{bmatrix}$
LW Spar	LW Root	Either	R^{LWR}_{LWS}	$\begin{bmatrix} 0 & 0 & -1 \\ -\sin\phi_{LW} & -\cos\phi_{LW} & 0 \\ -\cos\phi_{LW} & \sin\phi_{LW} & 0 \end{bmatrix}$
RW Planform Upstroke	RW Spar	Up	R^{RWS}_{RWPU}	$\begin{bmatrix} -\cos\alpha & 0 & \sin\alpha \\ 0 & 1 & 0 \\ -\sin\alpha & 0 & -\cos\alpha \end{bmatrix}$
RW Planform Downstroke	RW Spar	Down	R^{RWS}_{RWPD}	$\begin{bmatrix} \cos\alpha & 0 & \sin\alpha \\ 0 & 1 & 0 \\ -\sin\alpha & 0 & \cos\alpha \end{bmatrix}$
LW Planform Upstroke	LW Spar	Up	R^{LWS}_{LWPU}	$\begin{bmatrix} \cos\alpha & 0 & \sin\alpha \\ 0 & 1 & 0 \\ -\sin\alpha & 0 & \cos\alpha \end{bmatrix}$
LW Planform Downstroke	LW Spar	Down	R^{LWS}_{LWPD}	$\begin{bmatrix} -\cos\alpha & 0 & \sin\alpha \\ 0 & 1 & 0 \\ -\sin\alpha & 0 & -\cos\alpha \end{bmatrix}$

Table 2. Transformation Matrices.

III. Aerodynamic Model of Flapping Wing Vehicle with Independently Actuated Wings

A. Instantaneous Aerodynamic Forces and Centers of Pressure in Wing Planform Frames

The aerodynamic forces are derived, using blade element theory, for triangular shaped wings that have two degrees of freedom, namely, angular displacement, $\phi(t)$, about the wing root in the stroke plane, and angular displacement of the planform about the passive rotation hinge joint, which is equivalent to wing angle-of-attack, α, in still air. The triangular planform wing, shown in Figure 4, is taken to be a rigid flat plate whose elemental lift and drag at a spanwise location y_{WP} is given by:

$$dL = \frac{\rho}{2} C_L(\alpha) \dot{\phi}^2 y^2_{WP} c(y_{WP}) dy_{WP} \tag{1}$$

$$dD = \frac{\rho}{2} C_D(\alpha) \dot{\phi}^2 y_{WP}^2 c(y_{WP}) dy_{WP} \tag{2}$$

where $c(y_{WP})$ is the chord at the spanwise location y_{WP}, which is a location on the wing spar. Now compute the total lift and drag on the wing expressed in a wing planform fixed coordinate system, e.g., RWPU, RWPD, LWPU, and LWPD. Such a coordinate frame has an origin at the wing root hinge point and the x-y plane is coincident with the wing planform. The lift is computed by integrating the elemental lift over the span according to

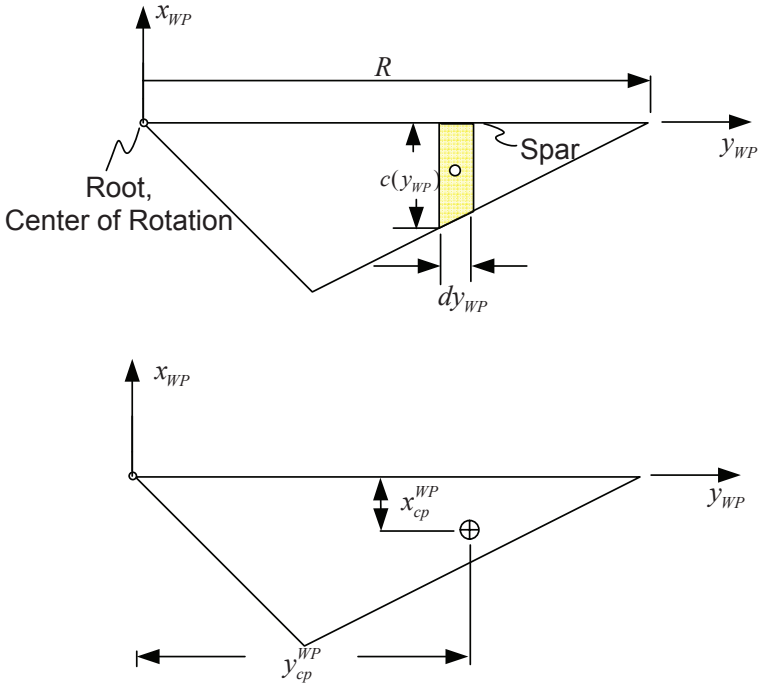

Figure 4. Blade element computation of aerodynamic forces, moments and centers of pressure.

$$L = \int_0^R dL = \frac{\rho}{2} C_L(\alpha) \dot{\phi}(t)^2 I_A \tag{3}$$

Similarly, drag is computed according to

$$D = \int_0^R dD = \frac{\rho}{2} C_D(\alpha) \dot{\phi}(t)^2 I_A \tag{4}$$

where I_A is the area moment of inertia of the planform about the root and R is the length of the wing. For convenience all of the time invariant parameters are lumped together according to

$$\begin{aligned} k_L &\triangleq \frac{\rho}{2} C_L(\alpha) I_A \\ k_D &\triangleq \frac{\rho}{2} C_D(\alpha) I_A \end{aligned} \tag{5}$$

thus, lift and drag can be expressed as the product of time invariant parameters and time varying functions

$$\begin{aligned} L &= k_L \dot{\phi}(t)^2 \\ D &= k_D \dot{\phi}(t)^2 \end{aligned} \tag{6}$$

The following expressions for lift and drag coefficients,[5] which were obtained from low Reynolds Number experiments, are used in this work

$$\begin{aligned} C_D(\alpha) &= 1.92 - 1.55\cos(2.04\alpha - 9.82) \\ C_L(\alpha) &= 0.225 + 1.58\sin(2.13\alpha - 7.2) \end{aligned} \tag{7}$$

where α is in degrees. Note that the only variable that can be actively manipulated to control the instantaneous aerodynamic forces is the angular velocity of the wing $\dot{\phi}(t)$ and that the forces are quadratic functions of this motion variable. The center of pressure in the plane of each wing must be obtained in order to compute moments on the fuselage. The center of pressure location for each wing in their respective local wing planform coordinate frame, namely RWPU, RWPD, LWPU, or LWPD, are:

$$x_{cp}^{WP} = \frac{\int_0^R y_{WP}^2 \frac{1}{2} c(y_{WP})^2 dy_{WP}}{\int_0^R y_{WP}^2 c(y_{WP}) dy_{WP}} = \frac{-c}{5}\left(\frac{3b^2 + 2bR + R^2}{b^2 + bR + R^2}\right) \tag{8}$$

$$y_{cp}^{WP} = \frac{\int_0^R y_{WP}^3 c(y_{WP}) dy_{WP}}{\int_0^R y_{WP}^2 c(y_{WP}) dy_{WP}} = \frac{3}{5}\left(\frac{b^3 + b^2R + bR^1 + R^3}{3b^2 + 2bR + R^2}\right) \tag{9}$$

$$z_{cp}^{WP} = 0 \tag{10}$$

where WP denotes any of the four local wing planform coordinate systems, b is the distance from the wing root to the wing break along the y_{WP} axis, and c is the maximum chord of this wing.

B. Expression of Aerodynamic Forces and Centers of Pressure in Body Frame

With the relationships between the body, roots, spars, upstroke planform and downstroke planform axis systems established in Tables 1 and 2, the instantaneous values of lift and drag on each wing are transformed into the body-axis coordinate frame. Recall that lift is defined as the component of aerodynamic force perpendicular to the relative wind, while drag is defined as the component of aerodynamic force parallel to the relative wind. If the air mass is quiescent, then the relative wind is parallel to the stroke plane, which is coincident with the x-y planes of the local spar-frames. Therefore, the lift and drag forces are conveniently expressed in the spar coordinate frames, which can be transformed to the

body frame using the rotation matrices defined in Table 2. For example, to express the aerodynamic force vector associated with the right wing on the upstroke in the body-frame, the following transformation is applied

$$\mathbf{F}^{B}_{RWU} = \mathbf{R}^{B}_{RWR}\mathbf{R}^{RWR}_{RWS}\mathbf{F}^{RWS}_{RWU} \tag{11}$$

The aerodynamic forces associated with each wing and stroke expressed in both the spar and body frames are summarized in Table 3.

Force	Local Spar Frame	Body Frame
RW Upstroke	$\mathbf{F}^{RWS}_{RWU} = \begin{bmatrix} D_{RWU} \\ 0 \\ -L_{RWU} \end{bmatrix}$	$\mathbf{F}^{B}_{RWU} = \begin{bmatrix} L_{RWU} \\ -D_{RWU}\sin\phi_{RWU}(t) \\ D_{RWU}\cos\phi_{RWU}(t) \end{bmatrix}$
RW Downstroke	$\mathbf{F}^{RWS}_{RWD} = \begin{bmatrix} -D_{RWD} \\ 0 \\ -L_{RWD} \end{bmatrix}$	$\mathbf{F}^{B}_{RWD} = \begin{bmatrix} L_{RWD} \\ D_{RWD}\sin\phi_{RWD}(t) \\ -D_{RWD}\cos\phi_{RWD}(t) \end{bmatrix}$
LW Upstroke	$\mathbf{F}^{LWS}_{LWU} = \begin{bmatrix} -D_{LWU} \\ 0 \\ -L_{LWU} \end{bmatrix}$	$\mathbf{F}^{B}_{LWU} = \begin{bmatrix} L_{LWU} \\ D_{LWU}\sin\phi_{LWU}(t) \\ D_{LWU}\cos\phi_{LWU}(t) \end{bmatrix}$
LW Downstroke	$\mathbf{F}^{LWS}_{LWD} = \begin{bmatrix} D_{LWD} \\ 0 \\ -L_{LWD} \end{bmatrix}$	$\mathbf{F}^{B}_{LWD} = \begin{bmatrix} L_{LWD} \\ -D_{LWD}\sin\phi_{LWD}(t) \\ -D_{LWD}\cos\phi_{LWD}(t) \end{bmatrix}$

Table 3. Aerodynamic forces expressed in local spar and body frames.

The center of pressure on each wing is conveniently expressed in the local wing planform frame associated with each stroke. To calculate the center of pressure in the body frame three coordinate frame rotations and one translation must be performed. One rotation is trivial because the root and body systems are parallel. The translation is associated with the distance between the origin of the body frame and the origin of each wing root frame. For example, for the right wing upstroke, the center of pressure location in the body frame is given by

$$\mathbf{r}_{\mathbf{cp}}{}^{B}_{RWU} = \mathbf{R}^{B}_{RWR}\mathbf{R}^{RWR}_{RWS}\mathbf{R}^{RWS}_{RWPU}\mathbf{r}_{\mathbf{cp}}{}^{RWPU}_{RWU} + \Delta\mathbf{r}^{B}_{R} \tag{12}$$

where $\Delta\mathbf{r}^{B}_{R}$ is the position vector from the origin of the body axes coordinate system to the

origin of the right wing root coordinate system, i.e.,

$$\begin{aligned}\Delta\mathbf{r}_R^B \triangleq \mathbf{r}_{o_{RWR}}^B &= \begin{bmatrix} \Delta x_R^B & \frac{w}{2} & \Delta z_R^B \end{bmatrix} \\ \Delta\mathbf{r}_L^B \triangleq \mathbf{r}_{o_{LWR}}^B &= \begin{bmatrix} \Delta x_L^B & -\frac{w}{2} & \Delta z_L^B \end{bmatrix}\end{aligned} \tag{13}$$

The width of the vehicle is designed as w and the origin of the body axis coordinate system is assumed to be located at the midpoint of the fuselage in the y-body axis direction. The centers of pressure associated with each wing and stroke, expressed in the body frame, are summarized in Table 4.

CP Location	Body Frame Expression
RW Upstroke	$\mathbf{r}_{\mathbf{cp}_{RWU}}^B = \begin{bmatrix} x_{cp}^{WP}\sin\alpha + \Delta x_R^B \\ x_{cp}^{WP}\sin\phi_{RW}\cos\alpha + y_{cp}^{WP}\cos\phi_{RW} + \frac{w}{2} \\ -x_{cp}^{WP}\cos\phi_{RW}\cos\alpha + y_{cp}^{WP}\sin\phi_{RW} + \Delta z_R^B \end{bmatrix}$
RW Downstroke	$\mathbf{r}_{\mathbf{cp}_{RWD}}^B = \begin{bmatrix} x_{cp}^{WP}\sin\alpha + \Delta x_R^B \\ -x_{cp}^{WP}\sin\phi_{RW}\cos\alpha + y_{cp}^{WP}\cos\phi_{RW} + \frac{w}{2} \\ x_{cp}^{WP}\cos\phi_{RW}\cos\alpha + y_{cp}^{WP}\sin\phi_{RW} + \Delta z_R^B \end{bmatrix}$
LW Upstroke	$\mathbf{r}_{\mathbf{cp}_{LWU}}^B = \begin{bmatrix} x_{cp}^{WP}\sin\alpha + \Delta x_L^B \\ -x_{cp}^{WP}\sin\phi_{LW}\cos\alpha - y_{cp}^{WP}\cos\phi_{LW} - \frac{w}{2} \\ -x_{cp}^{WP}\cos\phi_{LW}\cos\alpha + y_{cp}^{WP}\sin\phi_{LW} + \Delta z_L^B \end{bmatrix}$
LW Downstroke	$\mathbf{r}_{\mathbf{cp}_{LWD}}^B = \begin{bmatrix} x_{cp}^{WP}\sin\alpha + \Delta x_L^B \\ x_{cp}^{WP}\sin\phi_{LW}\cos\alpha - y_{cp}^{WP}\cos\phi_{LW} - \frac{w}{2} \\ x_{cp}^{WP}\cos\phi_{LW}\cos\alpha + y_{cp}^{WP}\sin\phi_{LW} + \Delta z_L^B \end{bmatrix}$

Table 4. Centers of pressure expressed in body frame.

IV. Aerodynamic Moments in Body Frame

The expressions for the aerodynamic moments associated with each wing and stroke are given by

$$\begin{aligned}\mathbf{M}_{RWU}^B &= \mathbf{r}_{\mathbf{cp}_{RWU}}^B \times \mathbf{F}_{RWU}^B \\ \mathbf{M}_{RWD}^B &= \mathbf{r}_{\mathbf{cp}_{RWD}}^B \times \mathbf{F}_{RWD}^B \\ \mathbf{M}_{LWU}^B &= \mathbf{r}_{\mathbf{cp}_{LWU}}^B \times \mathbf{F}_{LWU}^B \\ \mathbf{M}_{LWD}^B &= \mathbf{r}_{\mathbf{cp}_{LWD}}^B \times \mathbf{F}_{LWD}^B\end{aligned} \tag{14}$$

Carrying out the cross product operations and substituting the values from Tables 3 and 4 into the expressions in Equation 14 yields

$$\mathbf{M}^B_{RWU} = \begin{bmatrix} D_{RWU}\left[y^{WP}_{cp} + \frac{w}{2}\cos\phi_{RW} + \Delta z^B_R \sin\phi_{RW}\right] \\ \left\{L_{RWU}\left[y^{WP}_{cp}\sin\phi_{RW} + \Delta z^B_R\right] - D_{RWU}\Delta x^B_R \cos\phi_{RW} - \ldots \right. \\ \left. \left[L_{RWU}\cos\alpha + D_{RWU}\sin\alpha\right] x^{WP}_{cp}\cos\phi_{RW}\right\} \\ \left\{-D_{RWU}\Delta x^B_R \sin\phi_{RW} - L_{RWU}\left[\frac{w}{2} + y^{WP}_{cp}\cos\phi_{RW}\right] - \ldots \right. \\ \left. \left[L_{RWU}\cos\alpha + D_{RWU}\sin\alpha\right] x^{WP}_{cp}\sin\phi_{RW}\right\} \end{bmatrix} \tag{15}$$

$$\mathbf{M}^B_{RWD} = \begin{bmatrix} -D_{RWD}\left[y^{WP}_{cp} + \frac{w}{2}\cos\phi_{RW} + \Delta z^B_R \sin\phi_{RW}\right] \\ \left\{L_{RWD}\left[y^{WP}_{cp}\sin\phi_{RW} + \Delta z^B_R\right] + D_{RWD}\Delta x^B_R \cos\phi_{RW} + \ldots \right. \\ \left. \left[L_{RWD}\cos\alpha + D_{RWD}\sin\alpha\right] x^{WP}_{cp}\cos\phi_{RW}\right\} \\ \left\{D_{RWD}\Delta x^B_R \sin\phi_{RW} - L_{RWD}\left[\frac{w}{2} + y^{WP}_{cp}\cos\phi_{RW}\right] + \ldots \right. \\ \left. \left[L_{RWD}\cos\alpha + D_{RWD}\sin\alpha\right] x^{WP}_{cp}\sin\phi_{RW}\right\} \end{bmatrix} \tag{16}$$

$$\mathbf{M}^B_{LWU} = \begin{bmatrix} D_{LWU}\left[-y^{WP}_{cp} - \frac{w}{2}\cos\phi_{LW} - \Delta z^B_L \sin\phi_{LW}\right] \\ \left\{L_{LWU}\left[y^{WP}_{cp}\sin\phi_{LW} + \Delta z^B_L\right] - D_{LWU}\Delta x^B_L \cos\phi_{LW} - \ldots \right. \\ \left. \left[L_{LWU}\cos\alpha + D_{LWU}\sin\alpha\right] x^{WP}_{cp}\cos\phi_{LW}\right\} \\ \left\{D_{LWU}\Delta x^B_L \sin\phi_{LW} + L_{LWU}\left[\frac{w}{2} + y^{WP}_{cp}\cos\phi_{LW}\right] + \ldots \right. \\ \left. \left[L_{LWU}\cos\alpha + D_{LWU}\sin\alpha\right] x^{WP}_{cp}\sin\phi_{LW}\right\} \end{bmatrix} \tag{17}$$

$$\mathbf{M}^B_{LWD} = \begin{bmatrix} D_{LWD}\left[y^{WP}_{cp} + \frac{w}{2}\cos\phi_{LW} + \Delta z^B_L \sin\phi_{LW}\right] \\ \left\{L_{LWD}\left[y^{WP}_{cp}\sin\phi_{LW} + \Delta z^B_L\right] + D_{LWD}\Delta x^B_L \cos\phi_{LW} + \ldots \right. \\ \left. \left[L_{LWD}\cos\alpha + D_{LWD}\sin\alpha\right] x^{WP}_{cp}\cos\phi_{LW}\right\} \\ \left\{-D_{LWD}\Delta x^B_L \sin\phi_{LW} + L_{LWD}\left[\frac{w}{2} + y^{WP}_{cp}\cos\phi_{LW}\right] - \ldots \right. \\ \left. \left[L_{LWD}\cos\alpha + D_{LWD}\sin\alpha\right] x^{WP}_{cp}\sin\phi_{LW}\right\} \end{bmatrix} \tag{18}$$

Equations 15-18 provide the expressions for the instantaneous aerodynamic moments generated by each wing at any point in a wing beat cycle in the body-axis coordinate frame.

V. Split-Cycle Constant-Period Frequency Modulation Control Strategy

Because the vehicle is designed to mimic dipterian insect flight, $\dot{\phi}$ must be a time varying function that is equal to zero at the extreme limits of wing position. It is assumed that the wing position in the stroke plane can be controlled directly via a high bandwidth piezoelectric bimorph actuator. This assumption approximates the physics of applying a voltage to a

bimorph piezoelectric actuator that imparts rotational motion to a wing via a linkage that consists of rigid elements connected by pin joints. The forcing function that drives the rotation of each wing is selected as

$$\phi = \cos \omega t \tag{19}$$

As defined in Figure 3, the maximum value of this angle occurs when either wing reaches its maximum displacement towards the ventral side of the vehicle. Assuming that the frequency of the oscillating wing is held constant over the segment of interest for each wingbeat cycle, the angular velocity of the wing is given by

$$\dot{\phi} = -\omega \sin \omega t \tag{20}$$

Note that the units of ϕ are in radians and that the amplitude of the wing rotation in the stroke plane is taken to be ± 1 rad, which closely approximates the rotation limits used in the Harvard RoboFly. The frequency of the oscillator that drives the actuator is selected as the control input variable to enable multi-degree-of-freedom flight, and this frequency is allowed to change at key points in the wingbeat cycle, namely at the ends of the stroke when $\phi = 1, \dot{\phi} = 0$ and $\phi = -1, \dot{\phi} = 0$. In a companion paper concerning 1 degree-of-freedom (DOF) flight,[4] it was shown that, if the wingbeat frequency is held constant over each cycle, then the cycle-averaged longitudinal force along the x-body axis was always finite and positive, while the cycle-averaged z-body force was always zero. Such conditions made it possible to achieve a practical condition that approximates hover[4] and allows altitude tracking; however, in order to enable a vehicle to achieve multi-DOF flight, an additional control input variable must be introduced. In the interest of maintaining the simplicity of the actuation system, the controllability of a vehicle equipped only with independently actuated wings with passive rotation about the chord is examined. In order to achieve a non-zero time averaged body force in the z-direction, subject to the imposed actuation constraint, the blade element velocities must be asymmetric over the wing beat cycle. Although there are many ways to accomplish this, the waveforms that define the motion of the wing in the stroke plane are parameterized such that the frequencies of the upstroke and downstroke can be modified while maintaining the original period. This technique is called Split-Cycle Constant-Period Frequency Modulation. Each wing will be driven by a position command of the following form

$$\phi_U(t) = \cos\left[(\omega - \delta)t\right], \quad 0 \leq t < \tfrac{\pi}{(\omega-\delta)} \tag{21}$$

$$\phi_D(t) = \cos\left[(\omega + \sigma)t + \xi\right], \quad \tfrac{\pi}{(\omega-\delta)} \leq t < \tfrac{2\pi}{\omega} \tag{22}$$

where the $\phi_U(t)$ and $\phi_D(t)$ represent the angular position command associated with a given wing on the upstroke and downstroke, respectively, δ is the split-cycle parameter,

$$\sigma \triangleq \frac{\delta\omega}{\omega - 2\delta} \tag{23}$$

and the phase shift on downstroke is given by

$$\xi = \frac{-2\pi\delta}{\omega - 2\delta} \tag{24}$$

The phase shift enforces the compatibility condition where the frequency of the waveform changes, i.e.,

$$(\omega + \sigma)t|_{t=\frac{\pi}{\omega-\delta}} + \xi = \pi \tag{25}$$

Note that the split-cycle parameter, δ, and the fundamental frequency, ω, are control input variables and that σ is defined such that the wing beat cycle is completed at exactly the same time as it would be if the wing beat were temporally symmetric, i.e., $\delta = \sigma = 0$. The angular velocity of each wing over each split-cycle interval is given by

$$\dot{\phi}_U(t) = -(\omega - \delta)\sin\left[(\omega - \delta)t\right], \quad 0 \le t < \tfrac{\pi}{(\omega-\delta)} \tag{26}$$

$$\dot{\phi}_D(t) = -(\omega + \sigma)\sin\left[(\omega + \sigma)t + \xi\right], \quad \tfrac{\pi}{(\omega-\delta)} \le t < \tfrac{2\pi}{\omega} \tag{27}$$

VI. Cycle-Averaging

The control strategies proposed in this paper are based on the assumption that the bandwidth of the fuselage controller is much less than the trim flapping frequency required for hover. If a non-oscillatory control force and inertial measurements were available for feedback, one could use conventional control design techniques to synthesize feedback control laws that produce favorable closed loop responses. Here, time varying high frequency oscillatory control inputs must be used; therefore, the relationship between the cycle-averaged forces and moments and the control input parameters, namely ω_{LW}, δ_{LW}, ω_{RW} and δ_{RW}, which are the fundamental frequency and split-cycle parameters for the left and right wings, respectively, are computed. Feedback control laws based on cycle-averaged forces and moments will allow a vehicle to track desired angular and spatial positions in a mean sense; however, because of the true periodic nature of the aerodynamic forces, the vehicle will exhibit limit cycle behavior in a neighborhood about the mean position. The objective of this work is to develop controllers that drive the vehicle to a desired mean position and orientation.

The general method used to compute the cycle-averaged aerodynamic forces and their sensitivities to variations in the control input parameters will now be described. Define

$G(t)$ to be a generalized force aligned with a principal body-axis direction that may represent either a force or a moment. In order to compute the cycle-averaged generalized force associated with each wing, an integral of the following form is evaluated

$$\overline{G} = \frac{\omega}{2\pi} \int_0^{\frac{2\pi}{\omega}} G(t)dt \tag{28}$$

Since the introduction of the split-cycle parameter changes the frequency of the cosine wave when $(\omega - \delta)t = \pi$ in each cycle, it is convenient to split the integral as follows

$$\overline{G} = \frac{\omega}{2\pi} \left[\int_0^{\frac{\pi}{\omega-\delta}} G(\phi_U(t))dt + \int_{\frac{\pi}{\omega-\delta}}^{\frac{2\pi}{\omega}} G(\phi_D(t))dt \right] \tag{29}$$

The control derivatives associated with a generalized time-averaged force are calculated by computing the partial derivative with respect to each control input variable about the hover frequency ω_o.

$$\overline{G}_{\Delta\omega_l} = \left. \frac{\partial \overline{G}}{\partial \omega_l} \right|_{\omega_l=\omega_o,\delta_l=0} \tag{30}$$

$$\overline{G}_{\delta_l} = \left. \frac{\partial \overline{G}}{\partial \delta_l} \right|_{\omega_l=\omega_o,\delta_l=0} \tag{31}$$

$$\overline{G}_{\Delta\omega_r} = \left. \frac{\partial \overline{G}}{\partial \omega_r} \right|_{\omega_r=\omega_o,\delta_r=0} \tag{32}$$

$$\overline{G}_{\delta_r} = \left. \frac{\partial \overline{G}}{\partial \delta_r} \right|_{\omega_r=\omega_o,\delta_r=0} \tag{33}$$

These control derivatives will ultimately be used to design the control allocation portion of a 6 DOF control law for the flapping wing MAV.

VII. Definite Integrals for Computation of Time Averaged Aerodynamic Forces and Moments

In order to calculate the cycle-averaged forces and moments, it will be necessary to evaluate numerous integrals. Many have no indefinite integral solutions. For example, many of the integrands will be of the form $\cos(\cos\omega t)$ or $\sin(\cos\omega t)$. These terms arise because of the coordinate transformations of forces from local frames to the body frame and because of the fact that a cosine function was chosen to drive the position of the wing. Fortunately, definite integrals involving such functions exist over the intervals of interest for the present problem and can be derived from results presented in Gradshteyn & Ryzhik.[6] The solution

of many of these definite integrals involve a Bessel function of the first kind, $J_1(x)$, as well as Struve functions. The integrals involving Struve functions evaluate to zero over the limits of integration that arise in the formulation of this particular problem. For convenience, the solutions to the definite integrals that are required to compute the cycle-averaged forces and moments are provided below.

$$I_1 \triangleq \int_0^{\frac{\pi}{\omega-\delta}} \sin^2\left[(\omega-\delta)t\right] dt = \frac{\pi}{2(\omega-\delta)} \tag{34}$$

$$I_2 \triangleq \int_0^{\frac{\pi}{\omega-\delta}} \sin^2\left[(\omega-\delta)t\right] \sin\left(\cos\left[(\omega-\delta)t\right]\right) dt = 0 \tag{35}$$

$$I_3 \triangleq \int_0^{\frac{\pi}{\omega-\delta}} \sin^2\left[(\omega-\delta)t\right] \cos\left(\cos\left[(\omega-\delta)t\right]\right) dt = \frac{\pi J_1(1)}{(\omega-\delta)} \tag{36}$$

$$I_4 \triangleq \int_{\frac{\pi}{\omega-\delta}}^{\frac{2\pi}{\omega}} \sin^2\left[(\omega+\sigma)t+\xi\right] dt = \frac{\pi}{2(\omega+\sigma)} \tag{37}$$

$$I_5 \triangleq \int_{\frac{\pi}{\omega-\delta}}^{\frac{2\pi}{\omega}} \sin^2\left[(\omega+\sigma)t+\xi\right] \sin\left(\cos\left[(\omega+\sigma)t+\xi\right]\right) dt = 0 \tag{38}$$

$$I_6 \triangleq \int_{\frac{\pi}{\omega-\delta}}^{\frac{2\pi}{\omega}} \sin^2\left[(\omega+\sigma)t+\xi\right] \cos\left(\cos\left[(\omega+\sigma)t+\xi\right]\right) dt = \frac{\pi J_1(1)}{\omega+\sigma} \tag{39}$$

VIII. Cycle Averaged Forces

In this section, the cycle-averaged aerodynamic forces are evaluated. These forces are integrated with respect to time as each wing operates over an upstroke and downstroke. Later, the forces are used in the development of a control law by evaluating the change in cycle-averaged forces with respect to a change in the control input variables.

A. X Force

Substituting the expression for the instantaneous x-body force from Table 3 into Equation 29 produces

$$\overline{X}^B_{RW} = \frac{\omega_{RW}}{2\pi}\left[\int_0^{\frac{\pi}{\omega_{RW}-\delta_{RW}}} L_{RWU}(t)dt + \int_{\frac{\pi}{\omega_{RW}-\delta_{RW}}}^{\frac{2\pi}{\omega_{RW}}} L_{RWD}(t)dt\right] \tag{40}$$

Substituting Equations 6, 26, and 27 into Equation 40 yields

$$\begin{aligned}\overline{X}^B_{RW} =& \frac{k_L \omega_{RW}}{2\pi} \left[\int_0^{\frac{\pi}{\omega_{RW}-\delta_{RW}}} (\omega_{RW}-\delta_{RW})^2 \sin^2[(\omega_{RW}-\delta_{RW})t]dt + \right. \\ & \left. \int_{\frac{\pi}{\omega_{RW}-\delta_{RW}}}^{\frac{2\pi}{\omega_{RW}}} (\omega_{RW}+\sigma_{RW})^2 \sin^2[(\omega_{RW}+\sigma_{RW})t+\xi_{RW}]dt \right]\end{aligned} \tag{41}$$

Noting that the time varying functions under the integral signs are of the form I_1 and I_4 as given by Equations 34 and 37, respectively, Equation 41 can be written as

$$\overline{X}^B_{RW} = \frac{k_L \omega_{RW}}{2\pi} \left[(\omega_{RW}-\delta_{RW})^2 I_1 + (\omega_{RW}+\sigma_{RW})^2 I_4 \right] \tag{42}$$

or simply

$$\overline{X}^B_{RW} = \frac{k_L \omega_{RW}}{4} (2\omega_{RW} - \delta_{RW} + \sigma_{RW}) \tag{43}$$

Following a similar procedure for the left wing, it can be shown that

$$\overline{X}^B_{LW} = \frac{k_L \omega_{LW}}{4} (2\omega_{LW} - \delta_{LW} + \sigma_{LW}) \tag{44}$$

Note that both $\overline{X}^B_{RW}$ and $\overline{X}^B_{LW}$ are positive quantities. At a hover condition, where the x-body axis is normal to the surface of the earth, the forces produced by both wings act to counter the vehicle weight. It is also worthwhile to note that because of the geometric constraints imposed by the passive wing rotation joints shown in Figure 2, the instantaneous x-body force is always positive or zero which directs the force along the positive longitudinal axis of the vehicle.

B. Y Force

In order to compute the cycle-averaged y-body force for each wing, substitute the expression for the instantaneous y-body aerodynamic force from Table 3 into Equation 29 to obtain

$$\overline{Y}^B_{RW} = \frac{\omega_{RW}}{2\pi} \left[\int_0^{\frac{\pi}{\omega_{RW}-\delta_{RW}}} -D_{RWU}(t) \sin[\phi_{RW}(t)]dt + \int_{\frac{\pi}{\omega_{RW}-\delta_{RW}}}^{\frac{2\pi}{\omega_{RW}}} D_{RWD}(t) \sin[\phi_{RW}(t)]dt \right] \tag{45}$$

Substituting Equations 6, 21, 22, 26, and 27, into Equation 45 produces

$$\overline{Y}^{B}_{RW} = \frac{k_D \omega_{RW}}{2\pi} \left[- \int_0^{\frac{\pi}{\omega_{RW}-\delta_{RW}}} (\omega_{RW} - \delta_{RW})^2 \sin^2[(\omega_{RW} - \delta_{RW})t] \sin\left(\cos[(\omega_{RW} - \delta_{RW})t]\right) dt + \int_{\frac{\pi}{\omega_{RW}-\delta_{RW}}}^{\frac{2\pi}{\omega_{RW}}} (\omega_{RW} + \sigma_{RW})^2 \sin^2[(\omega_{RW} + \sigma_{RW})t + \xi_{RW}] \sin\left(\cos[(\omega_{RW} + \sigma_{RW})t + \xi_{RW}]\right) dt \right] \tag{46}$$

Noting that the time varying functions under the integral signs are of the form I_2 and I_5 as given by Equations 35 and 38 respectively, Equation 46 becomes

$$\overline{Y}^{B}_{RW} = 0 \tag{47}$$

Following a similar procedure for the left wing, it can be shown that

$$\overline{Y}^{B}_{LW} = 0 \tag{48}$$

Physically, this is a result of the fact that the component of drag pointing in the y-body direction points the same amount of time in the positive direction and at the same magnitude as it points in the negative y-body direction over the course of a wing beat cycle. Note that if a non-zero cycle-averaged force in the y direction were required, the frequency of the driving oscillator would have to be varied over finer intervals within each wing beat cycle. In other words, the wing beat frequency would have to be changed more than once per cycle.

C. Z Force

The calculation of the cycle-averaged force in the z-body direction follows a similar procedure. Substituting the expression for the instantaneous z-body aerodynamic force from Table 3 into Equation 29 we obtain:

$$\overline{Z}^{B}_{RW} = \frac{\omega_{RW}}{2\pi} \left[\int_0^{\frac{\pi}{\omega_{RW}-\delta_{RW}}} D_{RWU}(t) \cos[\phi_{RW}(t)] dt + \int_{\frac{\pi}{\omega_{RW}-\delta_{RW}}}^{\frac{2\pi}{\omega_{RW}}} -D_{RWD}(t) \cos[\phi_{RW}(t)] dt \right] \tag{49}$$

Substituting Equations 6, 21, 22, 26, and 27 into Equation 49 yields

$$\overline{Z}^B_{RW} = \frac{k_D \omega_{RW}}{2\pi} \left[\int_0^{\frac{\pi}{\omega_{RW}-\delta_{RW}}} (\omega_{RW} - \delta_{RW})^2 \sin^2[(\omega_{RW} - \delta_{RW})t] \cos\left(\cos[(\omega_{RW} - \delta_{RW})t]\right) dt - \int_{\frac{\pi}{\omega_{RW}-\delta_{RW}}}^{\frac{2\pi}{\omega_{RW}}} (\omega_{RW} + \sigma_{RW})^2 \sin^2[(\omega_{RW} + \sigma_{RW})t + \xi_{RW}] \cos\left(\cos[(\omega_{RW} + \sigma_{RW})t + \xi_{RW}]\right) dt \right] \tag{50}$$

Noting that the time-varying functions under the integral signs are of the form I_3 and I_6 as given by Equations 36 and 39 respectively, Equation 50 can be written as

$$\overline{Z}^B_{RW} = \frac{k_D \omega_{RW}}{2\pi} \left[(\omega_{RW} - \delta_{RW})^2 I_3 - (\omega_{RW} + \sigma_{RW})^2 I_6 \right] \tag{51}$$

or simply

$$\overline{Z}^B_{RW} = \frac{-k_D J_1(1) \omega_{RW}}{2} (\delta_{RW} + \sigma_{RW}) \tag{52}$$

Following a similar procedure for the left wing, it can be shown that

$$\overline{Z}^B_{LW} = \frac{-k_D J_1(1) \omega_{LW}}{2} (\delta_{LW} + \sigma_{LW}) \tag{53}$$

The result for the z-body axis is important because it means that nonzero cycle-averaged forces can indeed be generated and used to induce fore and aft linear accelerations. It can also be used to generate rolling moments.

IX. Cycle Averaged Moments

In this section, expressions for the cycle-averaged aerodynamic moments are derived. The cycle-averaged moments are later used in the development of a control law that requires an evaluation of the change in cycle-averaged moments with respect to a change in the control input variables.

A. Rolling Moment

Substituting the expression for the instantaneous x-body moment from Equations 15 and 16 into Equation 29 gives

$$\overline{M_x}^B_{RW} = \frac{\omega_{RW}}{2\pi} \left[\int_0^{\frac{\pi}{\omega_{RW}-\delta_{RW}}} M_{xRWU}(t) dt + \int_{\frac{\pi}{\omega_{RW}-\delta_{RW}}}^{\frac{2\pi}{\omega_{RW}}} M_{xRWD}(t) dt \right] \tag{54}$$

Substituting Equations 6, 21, 22, 26, and 27 into Equation 54 yields:

$$\begin{aligned}
\overline{M_x}^B_{RW} = \frac{\omega_{RW}}{2\pi}\Bigg[& k_D y_{cp}^{WP}(\omega_{RW}-\delta_{RW})^2 \int_0^{\frac{\pi}{\omega_{RW}-\delta_{RW}}} \sin^2[(\omega_{RW}-\delta_{RW})t]dt + \dots \\
& k_D\frac{w}{2}(\omega_{RW}-\delta_{RW})^2 \int_0^{\frac{\pi}{\omega_{RW}-\delta_{RW}}} \cos\left\{\cos\left[(\omega_{RW}-\delta_{RW})t\right]\right\}\sin^2[(\omega_{RW}-\delta_{RW})t]dt + \dots \\
& k_D\Delta z_R^B(\omega_{RW}-\delta_{RW})^2 \int_0^{\frac{\pi}{\omega_{RW}-\delta_{RW}}} \sin\left\{\cos\left[(\omega_{RW}-\delta_{RW})t\right]\right\}\sin^2[(\omega_{RW}-\delta_{RW})t]dt - \dots \\
& k_D(\omega_{RW}+\sigma_{RW})^2 y_{cp}^{WP} \int_{\frac{\pi}{\omega_{RW}-\delta_{RW}}}^{\frac{2\pi}{\omega_{RW}}} \sin^2\left[(\omega_{RW}+\sigma_{RW})t+\xi_{RW}\right]dt - \dots \\
& k_D(\omega_{RW}+\sigma_{RW})^2\frac{w}{2} \int_{\frac{\pi}{\omega_{RW}-\delta_{RW}}}^{\frac{2\pi}{\omega_{RW}}} \sin^2\left[(\omega_{RW}+\sigma_{RW})t+\xi_{RW}\right] \\
& \cos\left\{\cos\left[(\omega_{RW}+\sigma_{RW})t+\xi_{RW}\right]\right\}dt - \dots \\
& k_D(\omega_{RW}+\sigma_{RW})^2\Delta z_R^B \int_{\frac{\pi}{\omega_{RW}-\delta_{RW}}}^{\frac{2\pi}{\omega_{RW}}} \sin^2\left[(\omega_{RW}+\sigma_{RW})t+\xi_{RW}\right] \\
& \sin\left\{\cos\left[(\omega_{RW}+\sigma_{RW})t+\xi_{RW}\right]\right\}dt\Bigg]
\end{aligned} \tag{55}$$

Note that the integrals are of the form given in Equations 34 - 39; thus, Equation 55 can be written as

$$\begin{aligned}
\overline{M_x}^B_{RW} = \frac{\omega_{RW}k_D}{2\pi}\Big\{ & (\omega_{RW}-\delta_{RW})^2\left[y_{cp}^{WP}I_1 + \Delta z_R^B I_2 + \frac{w}{2}I_3\right] - \\
& (\omega_{RW}+\sigma_{RW})^2\left[y_{cp}^{WP}I_4 + \Delta z_R^B I_5 + \frac{w}{2}I_6\right]\Big\}
\end{aligned} \tag{56}$$

Substituting the results for the definite integrals, I_1 - I_6, and simplifying yields

$$\overline{M_x}^B_{RW} = -\frac{k_D\omega_{RW}(\delta_{RW}+\sigma_{RW})}{4}\left[y_{cp}^{WP} + wJ_1(1)\right] \tag{57}$$

Following a similar procedure for the left wing, it can be shown that

$$\overline{M_x}^B_{LW} = \frac{k_D\omega_{LW}(\delta_{LW}+\sigma_{LW})}{4}\left[y_{cp}^{WP} + wJ_1(1)\right] \tag{58}$$

Note that without split-cycle frequency modulation, i.e., $\delta_{RW} = \sigma_{RW} = \delta_{LW} = \sigma_{LW} = 0$, it would not be possible to generate non-zero cycle-averaged rolling moments on this aircraft. Thus, because of the constraints resulting from the minimally actuated vehicle design, split-cycle modulation is a sufficient condition for generating rolling control moments for the proposed aircraft.

B. Pitching Moment

The instantaneous y-body moment is determined by substituting Equations 15 and 16 into Equation 29

$$\overline{M_{y_{RW}}}^{B} = \frac{\omega_{RW}}{2\pi}\left[\int_{0}^{\frac{\pi}{\omega_{RW}-\delta_{RW}}} M_{y_{RWU}}(t)dt + \int_{\frac{\pi}{\omega_{RW}-\delta_{RW}}}^{\frac{2\pi}{\omega_{RW}}} M_{y_{RWD}}(t)dt\right] \tag{59}$$

Substituting Equations 6, 21, 22, 26, and 27 into Equation 59 yields:

$$\begin{aligned}
\overline{M_{y_{RW}}}^{B} = \frac{\omega_{RW}}{2\pi}\Bigg\{ & (\omega_{RW}-\delta_{RW})^2\left[k_L\Delta z_R^B\int_0^{\frac{\pi}{\omega_{RW}-\delta_{RW}}}\sin^2[(\omega_{RW}-\delta_{RW})t]dt \ + \ldots\right.\\
& -k_D\Delta x_R^B\int_0^{\frac{\pi}{\omega_{RW}-\delta_{RW}}}\sin^2[(\omega_{RW}-\delta_{RW})t]\cos\left\{\cos(\omega_{RW}-\delta_{RW})t\right\}dt + \ldots\\
& -k_L x_{cp}^{WP}\cos\alpha\int_0^{\frac{\pi}{\omega_{RW}-\delta_{RW}}}\sin^2[(\omega_{RW}-\delta_{RW})t]\cos\left\{\cos\left[(\omega_{RW}-\delta_{RW})t\right]\right\}dt + \ldots\\
& -k_D x_{cp}^{WP}\sin\alpha\int_0^{\frac{\pi}{\omega_{RW}-\delta_{RW}}}\sin^2[(\omega_{RW}-\delta_{RW})t]\cos\left\{\cos\left[(\omega_{RW}-\delta_{RW})t\right]\right\}dt + \ldots\\
& \left.k_L y_{cp}^{WP}\int_0^{\frac{\pi}{\omega_{RW}-\delta_{RW}}}\sin^2[(\omega_{RW}-\delta_{RW})t]\sin\left\{\cos\left[(\omega_{RW}-\delta_{RW})t\right]\right\}dt\right] + \ldots\\
& (\omega_{RW}+\sigma_{RW})^2\left[k_L\Delta z_R^B\int_{\frac{\pi}{\omega_{RW}-\delta_{RW}}}^{\frac{2\pi}{\omega_{RW}}}\sin^2\left[(\omega_{RW}+\sigma_{RW})t+\xi_{RW}\right]dt + \ldots\right.\\
& k_D\Delta x_R^B\int_{\frac{\pi}{\omega_{RW}-\delta_{RW}}}^{\frac{2\pi}{\omega_{RW}}}\sin^2\left[(\omega_{RW}+\sigma_{RW})t+\xi_{RW}\right]\\
& \cos\left\{\cos\left[(\omega_{RW}+\sigma_{RW})t+\xi_{RW}\right]\right\}dt \ + \ldots\\
& k_L x_{cp}^{WP}\cos\alpha\int_{\frac{\pi}{\omega_{RW}-\delta_{RW}}}^{\frac{2\pi}{\omega_{RW}}}\sin^2\left[(\omega_{RW}+\sigma_{RW})t+\xi_{RW}\right]\\
& \cos\left\{\cos\left[(\omega_{RW}+\sigma_{RW})t+\xi_{RW}\right]\right\}dt \ + \ldots\\
& k_D x_{cp}^{WP}\sin\alpha\int_{\frac{\pi}{\omega_{RW}-\delta_{RW}}}^{\frac{2\pi}{\omega_{RW}}}\sin^2\left[(\omega_{RW}+\sigma_{RW})t+\xi_{RW}\right]\\
& \cos\left\{\cos\left[(\omega_{RW}+\sigma_{RW})t+\xi_{RW}\right]\right\}dt \ + \ldots\\
& k_L y_{cp}^{WP}\int_{\frac{\pi}{\omega_{RW}-\delta_{RW}}}^{\frac{2\pi}{\omega_{RW}}}\sin^2\left[(\omega_{RW}+\sigma_{RW})t+\xi_{RW}\right]\\
& \left.\sin\left\{\cos\left[(\omega_{RW}+\sigma_{RW})t+\xi_{RW}\right]\right\}dt\right]\Bigg\}
\end{aligned} \tag{60}$$

Note that the integrals are of the form given in Equations 34 - 39; thus, Equation 60 can be written as

$$\begin{aligned}\overline{M}^B_{y_{RW}} =& \frac{\omega_{RW}}{2\pi}\left\{(\omega_{RW}-\delta_{RW})^2\left[k_L\Delta z^B_R I_1 - k_D\Delta x^B_R I_3 - k_L x^{WP}_{cp}\cos\alpha I_3 - \right.\right.\\ & k_D x^{WP}_{cp}\sin\alpha I_3 + k_L y^{WP}_{cp} I_2\left.\right] + (\omega_{RW}+\sigma_{RW})^2\left[k_L\Delta z^B_R I_4 + \right.\\ & \left.\left. k_D\Delta x^B_R I_6 + k_L x^{WP}_{cp}\cos\alpha I_6 + k_D x^{WP}_{cp}\sin\alpha I_6 + k_L y^{WP}_{cp} I_5\right]\right\}\end{aligned} \tag{61}$$

Substituting the results for the definite integrals, I_1 - I_6, and simplifying produces

$$\begin{aligned}\overline{M}^B_{y_{RW}} =& \frac{k_L\omega_{RW}}{2}\left[x^{WP}_{cp}J_1(1)\cos\alpha(\delta_{RW}+\sigma_{RW}) + \frac{\Delta z^B_R}{2}(2\omega_{RW}+\sigma_{RW}-\delta_{RW})\right] + \dots \\ & \frac{k_D J_1(1)\omega_{RW}}{2}\left\{(\delta_{RW}+\sigma_{RW})\left[x^{WP}_{cp}\sin\alpha + \Delta x^B_R\right]\right\}\end{aligned} \tag{62}$$

Following a similar procedure for the left wing, it can be shown that

$$\begin{aligned}\overline{M}^B_{y_{LW}} =& \frac{k_L\omega_{LW}}{2}\left[x^{WP}_{cp}J_1(1)\cos\alpha(\delta_{LW}+\sigma_{LW}) + \frac{\Delta z^B_L}{2}(2\omega_{LW}+\sigma_{LW}-\delta_{LW})\right] + \dots \\ & \frac{k_D J_1(1)\omega_{LW}}{2}\left\{(\delta_{LW}+\sigma_{LW})\left[x^{WP}_{cp}\sin\alpha + \Delta x^B_L\right]\right\}\end{aligned} \tag{63}$$

Note that without split-cycle frequency modulation, i.e., $\delta_{RW} = \sigma_{RW} = \delta_{LW} = \sigma_{LW} = 0$, there still exists a non-zero cycle-averaged pitching moment if $\Delta z^B_R \neq 0$ and $\Delta z^B_L \neq 0$. This result yields further insight into vehicle design for controllability. It suggests that the wing root hinge point should be placed such that its z-body location is coincident with the nominal vehicle center-of-gravity, i.e., $\Delta z^B_R = 0, \Delta z^B_L = 0$. Such an arrangement will yield a zero cycle-averaged pitching moment when the split-cycle parameters are zero, which is a desirable feature for maintaining hover. Note that the current Harvard RoboFly aircraft does not incorporate this feature and would immediately pitch forward if not constrained by the guide wires used in their experiment. Later, the effect of a bob-weight actuator, that can be used to manipulate pitching moments, will be examined.

C. Yawing Moment

The instantaneous z-body moment is determined by substituting Equations 15 and 16 into Equation 29 to obtain

$$\overline{M}^B_{z_{RW}} = \frac{\omega_{RW}}{2\pi}\left[\int_0^{\frac{\pi}{\omega_{RW}-\delta_{RW}}} M_{zRWU}(t)dt + \int_{\frac{\pi}{\omega_{RW}-\delta_{RW}}}^{\frac{2\pi}{\omega_{RW}}} M_{zRWD}(t)dt\right] \tag{64}$$

Substituting Equations 5, 21, 22, 26, and 27, into Equation 64 yields:

$$
\begin{aligned}
\overline{M}^{B}_{z_{RW}} = \frac{\omega_{RW}}{2\pi} \Bigg\{ (\omega_{RW} - \delta_{RW})^2 \Bigg[& -k_L \frac{w}{2} \int_0^{\frac{\pi}{\omega_{RW}-\delta_{RW}}} \sin^2[(\omega_{RW} - \delta_{RW})t] dt \ - \ldots \\
& k_D \Delta x^B_R \int_0^{\frac{\pi}{\omega_{RW}-\delta_{RW}}} \sin^2[(\omega_{RW} - \delta_{RW})t] \sin\left\{\cos(\omega_{RW} - \delta_{RW})t\right\} dt - \ldots \\
& k_L y^{WP}_{cp} \int_0^{\frac{\pi}{\omega_{RW}-\delta_{RW}}} \sin^2[(\omega_{RW} - \delta_{RW})t] \cos\left\{\cos\left[(\omega_{RW} - \delta_{RW})t\right]\right\} dt - \ldots \\
& k_L x^{WP}_{cp} \cos\alpha \int_0^{\frac{\pi}{\omega_{RW}-\delta_{RW}}} \sin^2[(\omega_{RW} - \delta_{RW})t] \sin\left\{\cos\left[(\omega_{RW} - \delta_{RW})t\right]\right\} dt - \ldots \\
& k_D x^{WP}_{cp} \sin\alpha \int_0^{\frac{\pi}{\omega_{RW}-\delta_{RW}}} \sin^2[(\omega_{RW} - \delta_{RW})t] \sin\left\{\cos\left[(\omega_{RW} - \delta_{RW})t\right]\right\} dt \Bigg] + \ldots \\
(\omega_{RW} + \sigma_{RW})^2 \Bigg[& -k_L \frac{w}{2} \int_{\frac{\pi}{\omega_{RW}-\delta_{RW}}}^{\frac{2\pi}{\omega_{RW}}} \sin^2\left[(\omega_{RW} + \sigma_{RW})t + \xi_{RW}\right] dt + \ldots \\
& k_D \Delta x^B_R \int_{\frac{\pi}{\omega_{RW}-\delta_{RW}}}^{\frac{2\pi}{\omega_{RW}}} \sin^2\left[(\omega_{RW} + \sigma_{RW})t + \xi_{RW}\right] \sin\left\{\cos\left[(\omega_{RW} + \sigma_{RW})t + \xi_{RW}\right]\right\} dt \ - \ldots \\
& k_L y^{WP}_{cp} \int_{\frac{\pi}{\omega_{RW}-\delta_{RW}}}^{\frac{2\pi}{\omega_{RW}}} \sin^2\left[(\omega_{RW} + \sigma_{RW})t + \xi_{RW}\right] \cos\left\{\cos\left[(\omega_{RW} + \sigma_{RW})t + \xi_{RW}\right]\right\} dt \ + \ldots \\
& k_L x^{WP}_{cp} \cos\alpha \int_{\frac{\pi}{\omega_{RW}-\delta_{RW}}}^{\frac{2\pi}{\omega_{RW}}} \sin^2\left[(\omega_{RW} + \sigma_{RW})t + \xi_{RW}\right] \\
& \sin\left\{\cos\left[(\omega_{RW} + \sigma_{RW})t + \xi_{RW}\right]\right\} dt \ + \ldots \\
& k_D x^{WP}_{cp} \sin\alpha \int_{\frac{\pi}{\omega_{RW}-\delta_{RW}}}^{\frac{2\pi}{\omega_{RW}}} \sin^2\left[(\omega_{RW} + \sigma_{RW})t + \xi_{RW}\right] \\
& \sin\left\{\cos\left[(\omega_{RW} + \sigma_{RW})t + \xi_{RW}\right]\right\} dt] \}
\end{aligned}
\tag{65}
$$

Note that the integrals are of the form given in Equations 34-39; thus, Equation 65 can be written as

$$
\begin{aligned}
\overline{M}^{B}_{z_{RW}} = & \frac{\omega_{RW}}{2\pi} \Big\{ (\omega_{RW} - \delta_{RW})^2 \Big[-k_L \frac{w}{2} I_1 - k_D \Delta x^B_R I_2 - k_L y^{WP}_{cp} I_3 - \\
& k_L x^{WP}_{cp} \cos\alpha I_2 - k_D x^{WP}_{cp} \sin\alpha I_2 \Big] + (\omega_{RW} + \sigma_{RW})^2 \Big[-k_L \frac{w}{2} I_4 + \\
& k_D \Delta x^B_R I_5 - k_L y^{WP}_{cp} I_6 + k_L x^{WP}_{cp} \cos\alpha I_5 + k_D x^{WP}_{cp} \sin\alpha I_5 \Big] \Big\}
\end{aligned}
\tag{66}
$$

Substituting the results for the definite integrals I_1-I_6, and simplifying yields

$$
\overline{M}^{B}_{z_{RW}} = \frac{-k_L \omega_{RW}}{2} \left[\left(y^{WP}_{cp} J_1(1) + \frac{w}{4} \right) (2\omega_{RW} - \delta_{RW} + \sigma_{RW}) \right] \tag{67}
$$

Following a similar procedure for the left wing, it can be shown that

$$\overline{M_z}^B_{LW} = \frac{k_L \omega_{LW}}{2} \left[\left(y_{cp}^{WP} J_1(1) + \frac{w}{4} \right) (2\omega_{RW} - \delta_{RW} + \sigma_{RW}) \right] \tag{68}$$

Without split-cycle frequency modulation, there exists a non-zero cycle-averaged yawing moment on each wing since $y_{cp}^{WP} \neq 0$ and $w \neq 0$. When the split-cycle parameters for each wing are zero, the cycle-averaged moments are opposing and balance one another. Since the fundamental wing beat frequency, ω, can be independently varied for each wing, yawing moments can be generated without varying the split-cycle parameters.

X. Summary

The analysis presented shows that the use of split-cycle constant-period frequency modulation, with independently actuated wings, allows manipulation the x-body and z-body axis forces. The y-body force is not directly controllable using the split-cycle approach as presented. Direct manipulation of the y-body force, given the physical design constraints of the proposed vehicle, would require that the frequency of the oscillators driving the wings be varied more than once per cycle. Rolling and yawing moments can also be independently varied using the split-cycle technique. A pitching moment can be generated; however, it cannot be generated independently of the z-body force or the rolling moment. In Part II, a bob-weight is introduced to cancel these undesirable changes in the pitching moment when manipulating the split-cycle parameters to generate z-body forces and rolling moments. Given the ability to independently manipulate 5 out of the 6 cycle-averaged body-axis forces and moments, untethered controlled flight with insect-like maneuverability appears to be feasible.

References

[1]Wood, R. J., "The First Takeoff of a Biologically Inspired At-Scale Robotic Insect," *IEEE Transactions on Robotics*, Vol. 24, No. 2, 2007, pp. 341–347.

[2]Ellington, C.P, "The Aerodynamics of Hovering Insect Flight. III. Kinematics," *Philosophical Transactions of the Royal Society of London*, Vol. B 305, 1984, pp. 41.

[3]Wood, R.J., Steltz E., and Fearing, R.S. , "Optimal Energy Density Piezoelectric Bending Actuators," *Sensors and Actuators A: Physical*, Vol. 119, 2005, pp. 476–488.

[4]Doman, D. B., Oppenheimer, M. W., Bolender, M. A., and Sigthorsson, D. O., "Altitude Control of a Single Degree of Freedom Flapping Wing Micro Air Vehicle," Submitted to 2009 AIAA Guidance, Navigation and Control Conference, Aug. 2009.

[5]Sane, S. P. and Dickenson, M. H., "The Control of Flight Force by a Flapping Wing: Lift and Drag Force Production," *The Journal of Experimental Biology*, Vol. 204, 2001, pp. 2607–2626.

[6]Gradshteyn, I.S. and Ryzhik, I.M., *Table of Integrals, Series and Products, 6 ed.*, Academic Press, 2000.